Development of an atomic clock for fission lifetime measurements

Kravchuk, Vladimir Leonidovich

6. Double coincidences analysis

In this section the analysis of coincidences between projectile-like fragments (PLF) and fission fragments (FF) will be described. The main purpose of this analysis is to determine the amount of PLF-FF coincidences for the reaction channels of interest. Following the procedure discussed in section 2.3 the quantity N_f, the number of fission events, and the number of x rays in coincidence with fission fragments N_{K-f} must be determined. These values are only meaningful for a particular reaction channel, i.e. in this way the normalization of the x-ray yield in each individual reaction channel can be obtained. The corresponding x-ray yield obtained from the triple coincidence analysis will be discussed in the next chapter. Gating on a certain reaction channel allows to determine the average excitation energy and angular momentum (see section 3.4).

6.1 Time analysis

The main purpose of the time analysis procedure is to determine the prompt coincident time window for the timing signals of the phoswich detectors and of the fission detectors. In figure 6.1 the time difference between a selected phoswich detector and one of the two fission detectors is shown. The FWHM= 4.5 ns of the prompt time peak originates from the variation in the time of flight. The prompt time window selection procedure was performed for all 52 (26 phoswich detectors and 2 fission detectors) individual time difference spectra. The position of the centroid of the prompt time peak was at most 1 ns shifted relative to all other time difference spectra. Also the position of the centroid was checked for the different runs and was found to be stable. The prompt time window gates from all spectra were selected for the further analysis.

In figure 6.2 the two-dimensional time spectrum (difference between time of the selected phoswich detector and the second fission detector versus difference between time of the selected phoswich detector and the first fission detector) is shown. There are five types of events presented in this plot. The intense diagonal line represents the prompt coincidences between the two fission detectors in random coincidences with the phoswich detector. The vertical (horizontal) line represents the prompt coincidences between

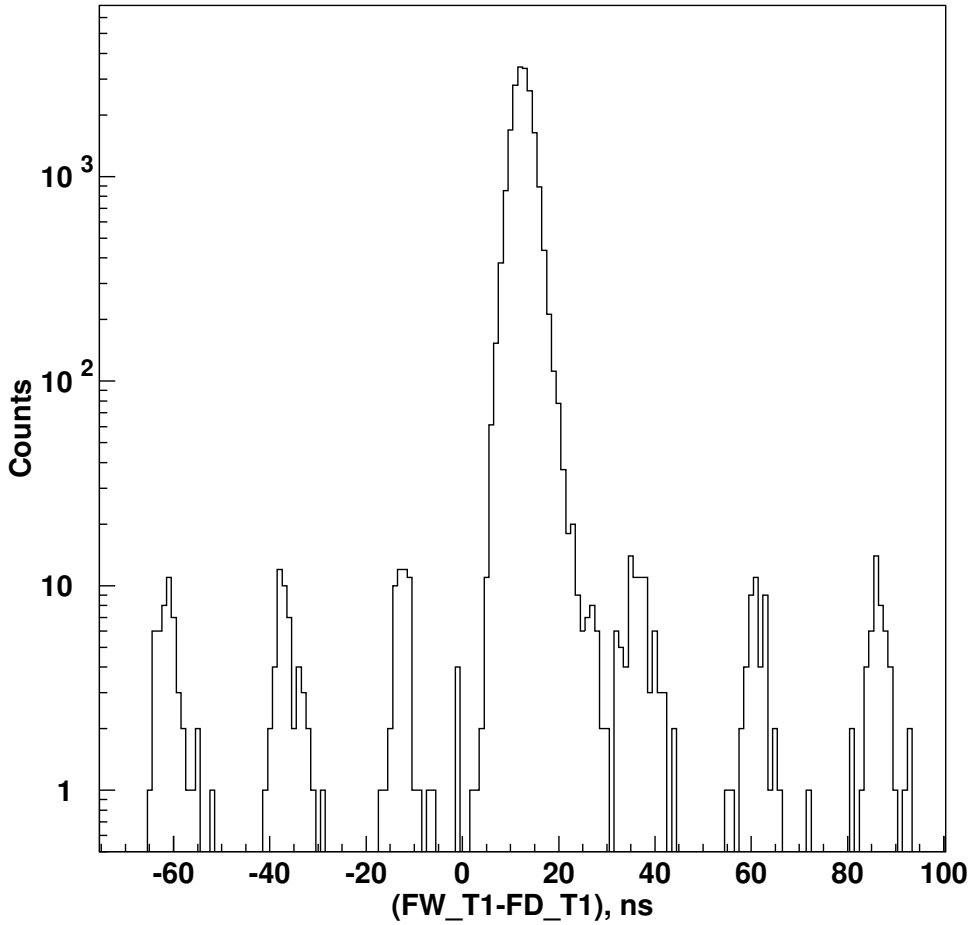

Figure 6.1: One-dimensional time difference spectrum for PLF-FF coincidences.

the phoswich detector and the first (second) fission detector in random coincidences with the second (first) fission detector. The crossing region of all three lines represents the true prompt coincidences between the phoswich detector and the fission detectors. Finally, the small amount of data points outside of each of the lines described above represents triple random coincidences.

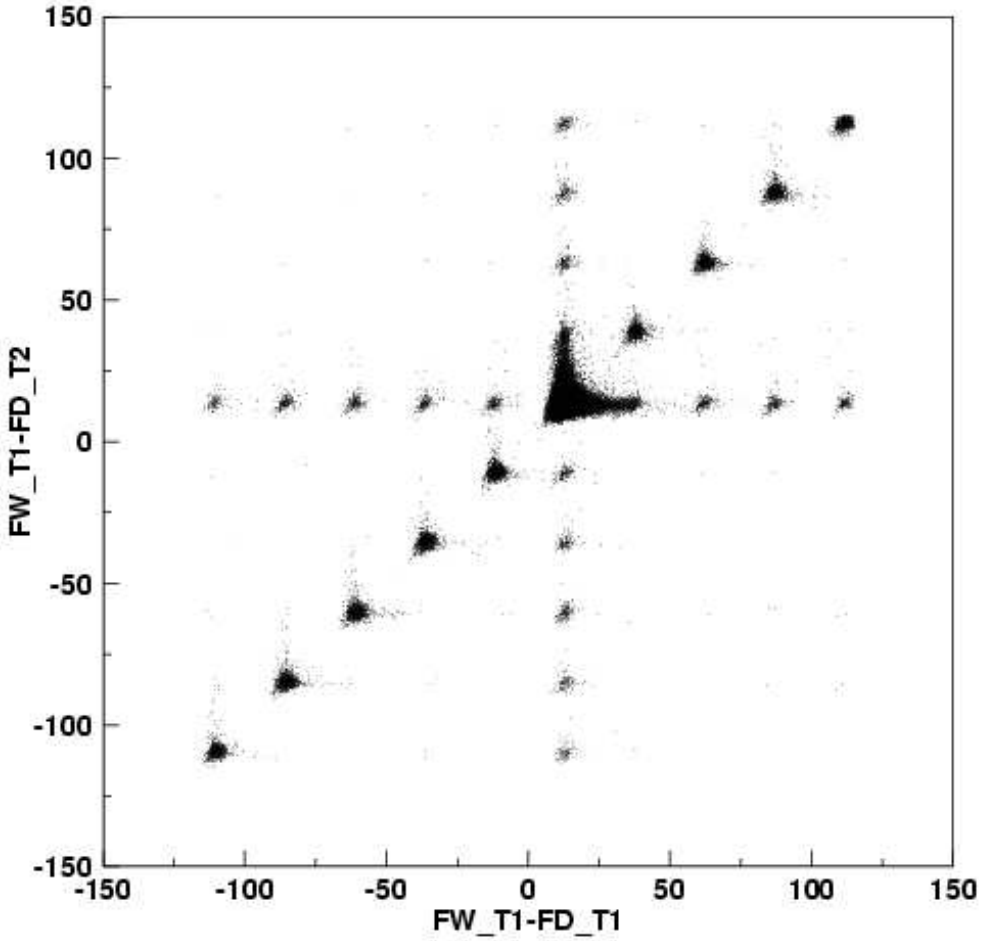

Figure 6.2: Two-dimensional three-fold time difference spectrum showing 5 types of coincident events (see text).

6.2 Selection of the fission fragments energy gate

In figure 5.11 of section 5.3 the inclusive and coincident energy spectra of the fission detector were shown. After gating on the prompt time window between the fission detectors, the low energy part of the coincidence spectrum

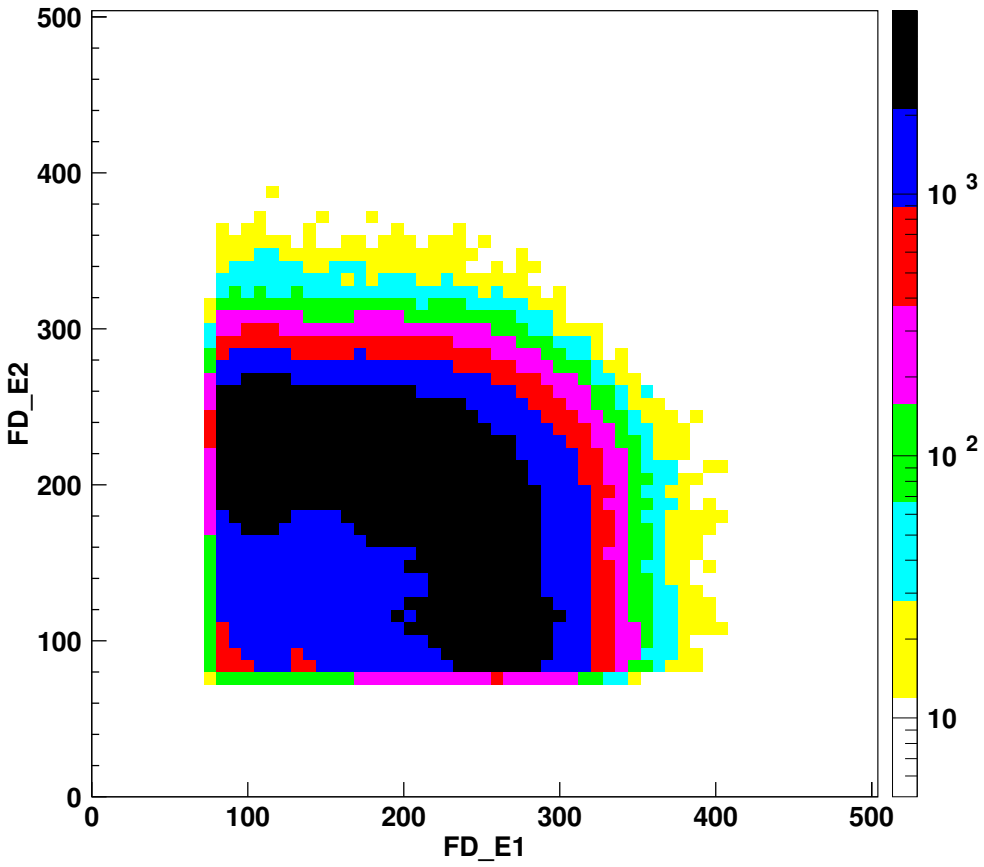

Figure 6.3: The two-dimensional plot representing energy of the second fission detector versus energy of the first fission detectors. The gate on the prompt coincidence window between the two fission detectors and the energy gates are applied.

changes sufficiently with respect to the inclusive spectrum. This indicates that energy gates have to be applied for both fission detectors in order to be above the electronic noise and small signals of the light charged particles, i.e. the energy gate on the true fission fragments has to be made. The two-dimensional spectrum of the correlation between the fission fragment energies is shown in figure 6.3. The energy gates larger then 75 channels

for both fission detectors are applied when producing this spectrum. The energy gates for the fission detectors described here are also used in the analysis of the triple coincidences with the x rays.

6.3 Partition of the cross section in reaction channels

The fission cross section is distributed over a large variety of reaction channels. In figure 6.4 the partition is shown for the channels including $Z \geq 5$ (top picture). The identification of channels in this plots is defined as

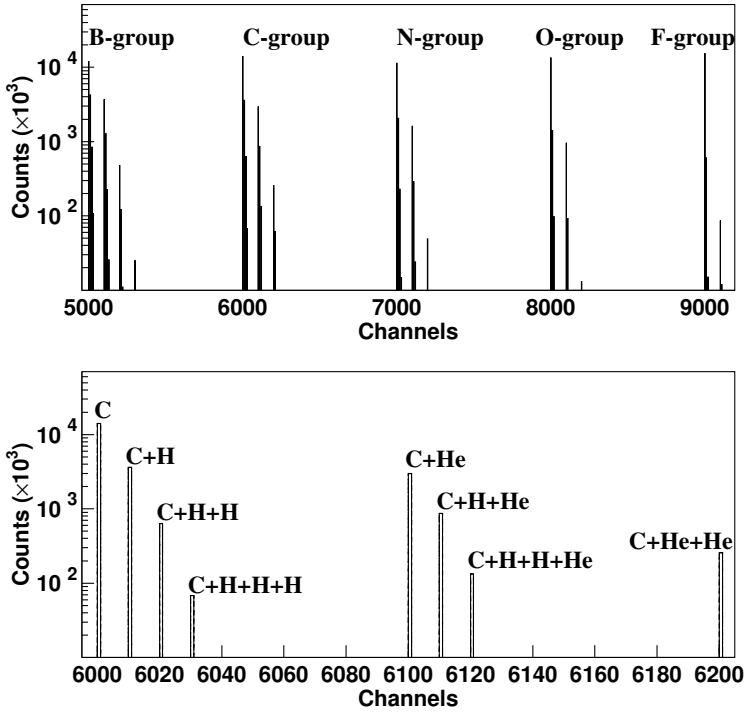

Figure 6.4: The charged-particle multiplicity plots. In the lower picture the zoomed region with the C-leading particle is shown. Reaction channels containing the C particles are indicated.

$$ch_{id} = 10^3 \times Z_{PLF} + 10^2 \times M_{He} + 10 \times M_H. \quad (6.1)$$

For example, the ch_{id} for the C+H+H+He reaction channel is 6120. In the bottom picture of figure 6.4 a zoomed region for channels including C is shown. Table 6.1 lists all observed reaction channels with their relative yields. The random subtraction was performed for all reaction channels. The higher limit for the random counts was found to be 1% of the prompts.

In the work of Leegte *et al.* [41] the 30 MeV/u ^{14}N + ^{232}Th reaction was studied. The partition of the fission cross section over 40 different reaction channels was presented. The comparison of the charged-particle multiplicities $M \leq 4$ obtained in this work and in [41] is shown in table 6.2. We can conclude that our relative yields follow those measured in [41], which had similar setup and reaction characteristics.

The coverage of the solid angle by the Mini Forward Wall detection system is incomplete. Therefore, reaction channels will be misidentified (for example, an O+He reaction channel with the He particle escaping detection is identified as an O reaction channel). The correction needed to obtain the actual partition is described in the following section

6.4 Correction to the reaction channel yields

A correction method was proposed in [41]. The main idea of the method is to correct for the particles which escaped detection due to incomplete coverage of the full solid angle by the detection system. If A_i^{meas} is the measured yield for reaction channel i we can write an equation

$$A_i^{meas} = \sum_j P_{ij} \cdot A_j^{true}. \quad (6.2)$$

Here P_{ij} is the probability to observe reaction channel j as reaction channel i. A_j^{true} is the true yield summed over all possible reaction channels, which can therefore be obtained using the inversion:

$$A_j^{true} = \sum_i P_{ij}^{-1} \cdot A_i^{meas}. \quad (6.3)$$

The probability matrix to observe reaction channel b_j out of a number of channels a_i containing all emitted particles is given, as suggested in [41], using a binomial distribution:

$$P_{ijZ} = \begin{pmatrix} a_i \\ b_j \end{pmatrix} \cdot \epsilon_{jZ}^{b_j} \cdot (1 - \epsilon_{jZ})^{a_i - b_j}. \quad (6.4)$$

Reaction channel	Relative yield, %
H	29.9
H+H	5.02
H+H+H	.668
H+H+H+H	.077
H+H+H+H+H	.008
He	21.6
He+He	3.44
He+He+He	.562
He+He+He+He	.071
He+He+He+He+He	.004
H+He	7.88
H+H+He	1.68
H+H+H+He	.272
H+H+H+H+He	.035
H+H+H+H+H+He	.003
H+He+He	1.66
H+H+He+He	.402
H+H+H+He+He	.065
H+H+H+H+He+He	.006
H+He+He+He	.267
H+H+He+He+He	.060
H+H+H+He+He+He	.008
H+H+H+H+He+He+He	.002
H+He+He+He+He	.029
H+H+He+He+He+He	.006
Li	2.58
Li+H	1.09
Li+H+H	.250
Li+H+H+H	.040
Li+H+H+H+H	.004
Li+He	1.01
Li+He+He	.223
Li+He+He+He	.026
Li+H+He	.476
Li+H+H+He	.101
Li+H+H+H+He	.016
Li+H+H+H+H+He	.002
Li+H+He+He	.100
Li+H+H+He+He	.018
Li+H+H+H+He+He	.001
Li+H+He+He+He	.009

Be	1.76
Be+H	.729
Be+H+H	.164
Be+H+H+H	.021
Be+H+H+H+H	.002
Be+He	.661
Be+He+He	.113
Be+He+He+He	.008
Be+H+He	.269
Be+H+H+He	.060
Be+H+H+H+He	.007
Be+H+He+He	.040
Be+H+H+He+He	.006
B	1.69
B+H	.573
B+H+H	.112
B+H+H+H	.015
B+H+H+H+H	.001
B+He	.495
B+He+He	.062
B+H+He	.172
B+H+H+He	.031
B+H+H+H+He	.003
B+H+He+He	.015
C	1.93
C+H	.481
C+H+H	.086
C+H+H+H	.009
C+He	.391
C+He+He	.033
C+H+He	.112
C+H+H+He	.016
N	1.57
N+H	.281
N+H+H	.031
N+H+H+H	.002
N+He	.211
N+H+He	.039

O	1.83
O+H	.199
O+H+H	.014
O+He	.131
F	2.11
F+H	.084
Ne	3.76

Table 6.1: Experimentally obtained partition of the cross section over observed reaction channels.

Charged-particle multiplicity	Relative yield , % (this work)	Relative yield, % (Leegte work)
$M = 1$	68.7	66.4
$M = 2$	22.7	26.1
$M = 3$	6.77	6.57
$M = 4$	1.31	.841

Table 6.2: Experimentally obtained partition of the cross section in charged-particle multiplicities compared with the results of Leegte [41].

In this equation ϵ_{jZ} is the efficiency to detect the particle of certain Z. To get the final probability matrix we are using the factorization of the probabilities, i.e.

$$P_{ij} = \prod_Z P_{ijZ}. \tag{6.5}$$

Let us show one example for P_{ijZ} and P_{ij}: If the reaction channel j is C+H and the primary channel i is C+H+H+H (2 particles C and H are present) then $b_j = 1$ and $a_i = 3$ and the probability matrix P_{ijH} is calculated as

$$P_{ijH} = \begin{pmatrix} 3 \\ 1 \end{pmatrix} \cdot \epsilon_H^1 \cdot (1 - \epsilon_H)^{3-1} = 3 \cdot \epsilon_H \cdot (1 - \epsilon_H)^2. \tag{6.6}$$

Trivially, in this case $P_{ijC} = \epsilon_C$. And, finally, the probability P_{ij} is

$$P_{ij} = P_{ijC} \cdot P_{ijH} = 3 \cdot \epsilon_C \cdot \epsilon_H \cdot (1 - \epsilon_H)^2, \tag{6.7}$$

i.e. the method relies on the empirically found factorization of cross sections (see also [41]). The main purpose of the application of this method in our

Reaction channel	Relative measured yield , %	Relative corrected yield, %
F-group		
F	96 ± 0.9	92 ± 3.5
F+H	4.0 ± 0.2	8.0 ± 1.3
O-group		
O	84 ± 0.8	64 ± 3.6
O+H	9.1 ± 0.2	16 ± 1.2
O+H+H	0.9 ± 0.1	3.0 ± 0.7
O+He	6.0 ± 0.2	17 ± 1.9
N-group		
N	74 ± 0.7	47 ± 3.9
N+H	13 ± 0.3	14 ± 1.0
N+H+H	1.4 ± 0.1	4.9 ± 0.9
N+H+H+H	0.1 ± .03	1.1 ± 0.4
N+H+He	1.8 ± 0.1	10 ± 2.0
N+He	9.9 ± 0.3	23 ± 1.4
C-group		
C	63 ± 0.6	36 ± 2.9
C+H	16 ± 0.3	12 ± 0.8
C+H+H	2.7 ± 0.1	3.7 ± 0.4
C+H+H+H	0.2 ± .02	2.4 ± 0.7
C+H+He	3.6 ± 0.1	15 ± 1.8
C+H+H+He	0.5 ± .05	6.1 ± 1.6
C+He	13 ± 0.2	16 ± 1.3
C+He+He	1.0 ± .07	8.8 ± 1.6

Table 6.3: Measured and corrected partition of the cross sections for F, O, N and C reaction channel groups.

case is to determine corrected yields for the reaction channels of interest like O+He, C+He+He *etc.* In [41] detection efficiencies for the Forward Wall detection system were explicitly measured. The values for detection H and He particles were found to be 0.70 and 0.65, respectively. Due to the smaller coverage of the solid angle by the Mini Forward Wall detection system the efficiencies in our case are smaller. It is also important to mention that we had a larger beam opening area in comparison with [41]. This has also an impact on the efficiency results as the angular distribution is different

for the H and He particles (see figures 5.1 and 5.3 of [40]). We determined efficiencies for the H and He particles by solving equation 6.3 and taking the minimum values for the efficiencies leading to positive yields in A_j^{true} as starting condition for a search. Next it was required that $\sigma_{M(i)} > \sigma_{M(i+1)}$, where σ is the corrected yield and M is the charged-particle multiplicity. Our efficiency results found this way are $\epsilon_H = 0.50$ for H particle detection and $\epsilon_{He} = 0.35$ for He particle detection. The systematic error in ϵ_H and ϵ_{He} is the main error in the corrected yield for most channels (see errors in the last column of table 6.3). Table 6.3 lists measured and corrected relative yields for the four groups of reaction channels: F-group, O-group, N-group and C-group (i.e. groups were F, O, N and C particles were detected). In table 6.4 the partition of the reaction channels is shown, when only one fragment (F, O, N or C) has been detected, i.e. we gate on the binary reaction channels and see the contribution of non-binary channels to the apparent binary reaction channel. Thus, 96, 77, 64 and 56 %, respectively, were due to a binary reaction. The errors are estimated to be less then 5 % for the binary channels and at least 10 % for other channels.

Using the corrected values of tables 6.3 and 6.4 one can calculate the relative partition for different Z_{TLF}. Table 6.5 lists the partition for different Z_{TLF} for two cases discussed above. The first case is where one gates on channels involving a leading particle (F-group, O-group, N-group, C-group). This is shown in the top four panels of table 6.5. The second case is when gating is done on F, O, N, or C only (lower four panels of table 6.5). The results listed in table 6.5 have the errors, which are following those in table 6.3 and discussion of the results in table 6.4 (see above). The best choice for observing binary transfer reactions is by gating on a single particle.

To summarize this chapter, we obtained the partition of the fission cross section over all observed reaction channels. The number of PLF-FF coincidences N_f is in the order of 10^7 for each of the main reaction channels. The partial cross section for the O channel, assuming the fission probability to be 1, is estimated to be 55 mb, which is 1.4 % of the total reaction cross section (4000 mb). Corrections were made using the method described above and the partition of the yield associated with different Z_{TLF} was determined. It was found that the most effective gate in triple coincidence analysis should be set on a single particle.

Reaction channel	Relative corrected yield, %
F	
F	96
F+H	4.0
O	77
O+H	9.3
O+H+H	0.7
O+He	13
N	
N	64
N+H	9.6
N+H+H	1.7
N+H+H+H	0.1
N+H+He	4.6
N+He	20
C	
C	56
C+H	10
C+H+H	1.4
C+H+H+H	0.5
C+H+He	7.6
C+H+H+He	1.6
C+He	17
C+He+He	5.9

Table 6.4: Partition of the reaction channels when only one fragment (F, O, N or C) has been detected (see text).

Reaction channel group	Z_{TLF}	Relative corrected yield, %
F-group	90	8.0
	91	92
O-group	90	20
	91	16
	92	64
N-group	90	11
	91	28
	92	14
	93	47
C-group	90	15
	91	17
	92	20
	93	12
	94	36
F	90	4.0
	91	96
O	90	14
	91	9.0
	92	77
N	90	4.5
	91	22
	92	9.5
	93	64
C	90	7.5
	91	8.5
	92	18
	93	10
	94	56

Table 6.5: Partition of the yield for different Z_{TLF} (see text).